

¹²³I-*iomazenil* whole-body imaging to detect hepatic carboxylesterase drug-metabolizing enzyme activity

Asuka Mizutani, MS ^{1,2}, Masato Kobayashi, PhD³, Ken-ichi Fujita, PhD⁴, Kotaro Takahashi⁵, MS, Tsuzumi Hokama, BS⁵, Hiroaki Takasu, BS⁵, Kodai Nishi, PhD⁶, Ryuichi Nishii, MD, PhD⁷, Naoto Shikano, PhD⁸, Kazuki Fukuchi, MD, PhD¹, Keiichi Kawai, PhD^{5,9,*}

¹ Division of Medical Technology and Science, Department of Medical Physics and Engineering, Course of Health Science, Graduate School of Medicine, Osaka University, Osaka, Japan

² Department of Radiology, Kanazawa University Hospital, Kanazawa, Japan

³ Wellness Promotion Science Center, College of Medical, Pharmaceutical and Health Sciences, Kanazawa University, Kanazawa, Japan

⁴ Institute of Molecular Oncology, Showa University, Tokyo, Japan

⁵ School of Health Sciences, College of Medical, Pharmaceutical and Health Sciences, Kanazawa University, Kanazawa, Japan

⁶ Department of Radioisotope Medicine, Atomic Bomb Disease Institute, Nagasaki University, Nagasaki, Japan

⁷ Molecular Imaging Center, National Institute of Radiological Sciences, Chiba, Japan

⁸ Department of Radiological Sciences, Ibaraki Prefectural University of Health Sciences, Ibaraki, Japan

⁹ Biomedical Imaging Research Center, University of Fukui, Fukui, Japan

Address correspondence and requests for reprints to:

Keiichi Kawai, PhD

School of Health Sciences, College of Medical, Pharmaceutical and Health Sciences,
Kanazawa University

5-11-80 Kodatsuno, Kanazawa 920-0942, Japan

Tel: +81-76-265-2527; Fax: +81-76-234-4366

E-mail: kei@mhs.mp.kanazawa-u.ac.jp

Abstract

Objectives: Drugs are mainly metabolized by hepatic enzymes, the activity of which can differ between individuals. Although it is ideal to measure the hepatic clearance of liver-targeted drugs in individualized medicine, blood enzyme tests typically measure metabolic drug clearance in the entire body, and not just in the liver. We investigated whether ^{123}I -iomazenil imaging can directly assess and quantify the activity of hepatic drug-metabolizing enzymes.

Methods: Hepatic enzymes that metabolize ^{123}I -iomazenil were identified by thin-layer chromatography in mouse liver homogenates with bis(4-nitrophenyl) phosphate (BNPP) inhibitor for carboxylesterase enzymes and nicotinamide adenine dinucleotide phosphate (NADPH) generator for cytochrome P450 enzymes. Whole-body images of mice were acquired using ^{123}I -iomazenil with and without BNPP, and the distribution was also obtained. The metabolism of ^{123}I -iomazenil in the blood, liver, gall bladder, and bladder was investigated by thin-layer chromatography.

Results: From the in-vitro metabolism of ^{123}I -iomazenil using BNPP, the enzyme converting ^{123}I -iomazenil to ^{123}I -R-COOH was identified as carboxylesterase, and that converting ^{123}I -iomazenil to M2 was identified as cytochrome P450 in experiments with and without an NADPH generator. The biological distribution and whole-body imaging showed increased accumulation in the liver of mice administered BNPP compared with normal mice, but decreased levels in the gall bladder and small intestine. The main fraction in bile and urine was ^{123}I -R-COOH, with two unknown metabolites (M1 and M2), $^{123}\text{I}^-$, and ^{123}I -iomazenil also being present.

Conclusions: ^{123}I -iomazenil whole-body imaging has good possibility of direct measurement of hepatic carboxylesterase activity as accumulation of ^{123}I -R-COOH in the gall bladder through bile and in the bladder through urine.

Keywords: ^{123}I -iomazenil, Whole-body imaging, Drug-metabolizing enzyme, Carboxylesterase, Individualized medicine

Introduction

Drugs are mainly metabolized in vivo by hepatic enzymes, the activity of which can differ between individuals [1,2], because of various factors such as genetic polymorphisms. This can lead to therapeutic failure, adverse effects, or drug toxicity [3–5]. The liver harbors many hepatic drug-metabolizing enzymes including cytochrome P450 (CYP) [6] and carboxylesterase [7,8]. Measuring the activity and capacity of hepatic drug-metabolizing enzymes could be useful for determining the best drug and

optimal dose to use in individualized medicine. Although it is ideal to measure the hepatic clearance of liver-targeted drugs [9] in individualized medicine, blood enzyme tests typically measure metabolic drug clearance in the entire body, and not just in the liver [3]. The in-vitro–in-vivo extrapolation method has been applied with human hepatic samples to measure metabolic drug clearance [10], but hepatic cells in vitro do not perfectly mimic cells in complete organs.

Nuclear medicine imaging could potentially be used to directly detect and quantify the activity of drug-metabolizing enzymes in metabolic drug clearance. To achieve this, however, the following conditions must be met: (i) a radiopharmaceutical accumulates in a metabolic organ, (ii) the radiopharmaceutical is metabolized by a specific drug-metabolizing enzyme and the radioactive metabolite transfers from the metabolic organ to an excretory organ, (iii) accumulation in the excretory organ can be visualized and quantitated. Our previous study showed that ^{123}I -*N*-isopropyl-*p*-iodoamphetamine (^{123}I -IMP), which is clinically used to measure cerebral blood flow in single-photon emission computed tomography (SPECT) imaging, [11–14] is mainly metabolized and converted to ^{123}I -*p*-iodoamphetamine in the liver by the specific enzyme CYP2C19 in humans [13]. We reported that chromatographic analysis of blood samples, not whole-body imaging, can be used to measure CYP2C19 activity in the human liver using ^{123}I -IMP, but this methodology also measures metabolic drug clearance in the entire body. Although whole-body imaging is a noninvasive method for the clinical analysis of enzyme activity, it is difficult to directly detect and quantify

CYP2C19 activity in ^{123}I -IMP whole-body imaging, because small amounts of administered ^{123}I -IMP are converted to ^{123}I -*p*-iodoamphetamine, a hepatic metabolite, by hepatic CYP2C19, as shown in our previous study [13].

^{123}I -Iomazenil (^{123}I -IMZ) has already been used for neural receptor scintigraphy in clinical examinations [15] and is primarily metabolized to a carboxylic acid (^{123}I -R-COOH), with deiodination (^{123}I -), limited conjugation (^{123}I -R-COOH-Glc), and oxidation (^{123}I -R'-CH₂COOH) (see Supplementary Fig., Supplemental digital content 1, <http://links.lww.com/NMC/A132>, which shows metabolic pathway of ^{123}I -IMZ) [16]. ^{123}I -IMZ accumulates in the bile, urine, and feces by enterohepatic and renal routes in both small animals [16] and humans [17–19]. Thus, ^{123}I -IMZ is a possible candidate for direct detection and quantification of the activity of drug-metabolizing enzymes based on the above necessary conditions. The objective of this study was to investigate whether ^{123}I -IMZ whole-body imaging enables detection and quantification of hepatic drug-metabolizing enzyme activity.

Methods

Materials

Acetate, chloroform, dipotassium hydrogen phosphate, EDTA disodium salt, glucose-6-phosphate, magnesium chloride, potassium dihydrogen phosphate, and sodium acetate were purchased from Nacalai Tesque (Kyoto, Japan). Bis(4-nitrophenyl) phosphate (BNPP) was purchased from Tokyo Chemical Industry (Tokyo, Japan). β -NADP⁺ and glucose-6-phosphate dehydrogenase (G6PD) were purchased from Oriental Yeast

(Osaka, Japan). ^{125}I -IMZ was supplied by and ^{123}I -IMZ was purchased from Nihon Medi-Physics (Chiba, Japan). The radiochemical purity of ^{123}I -IMZ and ^{125}I -IMZ was more than 98 and 95%, respectively. All of the other reagents and chemicals were of analytical or high-performance liquid chromatography grade.

Metabolism of ^{123}I -IMZ in vitro

To prepare the pooled liver homogenates, three 6-week-old male ddY mice (Japan SLC, Tokyo, Japan) were euthanized under anesthesia using isoflurane. The livers were removed and weighed. After addition of Krebs-Ringer phosphate buffer (pH = 7.4), the pooled livers were homogenized with an ultrasonic homogenizer (SONIFIER250; Branson, St. Luis, Missouri, USA), and the protein content was determined according to the bicinchoninic acid method [20]. For analysis of carboxylesterase-mediated metabolism, BNPP was used as a specific and hepatic carboxylesterase inhibitor [21]. Carboxylesterase-mediated metabolism of ^{123}I -IMZ was examined in a mixture consisting of 100 mmol/l sodium potassium phosphate buffer (pH = 7.4), 50 $\mu\text{mol/l}$ EDTA disodium salt, the nicotinamide adenine dinucleotide phosphate (NADPH)-generating system (0.5 mmol/l β -NADP⁺, 5 mmol/l MgCl_2 , 5 mmol/l glucose-6-phosphate, and 1 U/ml glucose-6-phosphate dehydrogenase), BNPP (0.1, 1, 10, 100 $\mu\text{mol/l}$), and 1000 μg protein/20 μl pooled mouse liver homogenates in a final volume of 250 μl . A mixture without BNPP was used as the control. The sample was incubated at 37°C for 60 min with gentle shaking. The reaction was stopped by adding 100 μl ethanol. Subsequently, the mixture was centrifuged for 5 min at 18 000g, and the

supernatant was analyzed by thin-layer chromatography (TLC) using chloroform/ acetate/H₂O at a ratio of 65 : 35 : 5 [22]. For analysis of CYP-mediated metabolism, NADPH was used as an energy source [6]. NADPH-dependent metabolism of ¹²³I-IMZ was examined in an incubation mixture consisting of 100 mmol/l sodium potassium phosphate buffer (pH = 7.4), 50 μmol/l EDTA disodium salt, NADPH generator, and 1000 μg protein/20 μl pooled mouse liver homogenates in a final volume of 250 μl. A mixture without NADPH generator was used as the control. The sample was incubated at 37°C for 60 min with gentle shaking. The reaction was stopped by adding 100 μl ethanol. Subsequently, the mixture was centrifuged for 5 min at 18 000g. The metabolites in each sample were analyzed by TLC. The supernatant was spotted onto a silica gel TLC plate 60 F254 (Merck, Darmstadt, Germany). The TLC plate and the TLC spots were developed using chloroform/acetate/H₂O at a ratio of 65 : 35 : 5 [22]. After development and complete drying, the TLC plates were cut into 21 fractions, and the radioactivity associated with each fraction was quantified using a γ-ray counter (AccuFLEXy 7000; Aloka, Tokyo, Japan). The fractional ratios of ¹²³I⁻, ¹²³I-R-COOH, ¹²³I-IMZ, and other metabolites were calculated by dividing the radioactive counts for each fraction by the total radioactivity count.

Whole-body imaging and biological distribution in normal mice using ^{123/125}I-IMZ

Animal studies were approved by the Animal Care Committee at Kanazawa University (Kanazawa, Japan) and were conducted in accordance

with international standards for animal welfare and institutional guidelines. All of the acquisitions were performed using a U-SPECT-II/CT system (MILabs, Utrecht, the Netherlands). Three normal mice were injected with 45 MBq of ^{123}I -IMZ by the tail vein. Whole-body SPECT images were acquired every 3 min from 15 to 60 min after injection under 2.0% isoflurane anesthesia. The images were reconstructed using ordered subset expectation maximization method with 16 subsets and six iterations including no scatter and attenuation correction. The voxel size was set to $0.8 \times 0.8 \times 0.8$ mm. A Gaussian filter with 1.0 mm was applied for post-reconstruction smoothing filtering. Image display was performed using medical image data analysis software, AMIDE (version 1.0.2) [23]. The coronal images were displayed as maximum intensity projection.

In biological distribution of normal mice, ^{125}I -IMZ was prepared to a specific activity of 185 kBq/ml by addition of saline. A total of 18 fasted mice were administered ^{125}I -IMZ by the tail vein (18.5 kBq/mouse). At 2, 5, 10, 30, 60, and 120 min, three normal mice were, respectively, euthanized under isoflurane, and the following tissues were collected: blood, brain, thyroid, lung, heart, stomach, liver, gall bladder, small intestine, large intestine, kidney, and bladder. Tissues were weighed, and radioactivity was quantified using an automated γ -ray counter to calculate the percent injected dose (%ID) or percent injected dose per gram of tissue (%ID/g).

Whole-body imaging and biological distribution in mice administered BNPP using $^{123/125}\text{I}$ -IMZ

Three mice were intraperitoneally injected with 100 mg/ kg BNPP.

After 30 min of BNPP injection, 45 MBq of ^{123}I -IMZ was injected by the tail vein. Whole-body SPECT images were acquired every 3 min from 15 to 60 min after ^{123}I -IMZ injection under 2.0% isoflurane anesthesia. Reconstruction method was the same with normal mice study.

In the biological distribution, a total of 18 mice were intraperitoneally injected with 50 or 100 mg/kg of BNPP at 30 min before injection of ^{125}I -IMZ. At 30, 60, and 120 min after ^{125}I -IMZ injection, three mice were, respectively, euthanized under isoflurane, and tissues were collected and quantified in the same manner as with the normal mice study.

Metabolism of ^{123}I -IMZ in vivo

^{123}I -IMZ was prepared to a specific activity of 30 MBq/ml by addition of saline. A total of 12 fasted mice were administered ^{123}I -IMZ by the tail vein (3.7 MBq/mouse). At 10, 30, 60, and 120 min, three mice, respectively, were euthanized under isoflurane, and the following tissues were collected: blood, liver, gall bladder, and bladder. The metabolites present in each tissue were analyzed by TLC. Briefly, bile and urine were directly spotted onto a TLC plate, and heparin was added to 300 μl blood and centrifuged for 5 min at 18 000g. Perchloric acid (30 μl) was added to the supernatant, which was centrifuged again, after which, the final supernatant was spotted onto the TLC plate as plasma. Krebs-Ringer phosphate buffer was added to the liver samples, followed by homogenization. Thereafter, ethanol was added to the homogenate to remove proteins, and the sample was centrifuged for 5 min at 18 000g. The final supernatant was analyzed by TLC using

chloroform/acetate/H₂O at a ratio of 65 : 35 : 5 [22].

Statistical analysis

Data were analyzed using Student's t-test, and P values less than 0.01 and 0.05 were considered statistically significant.

Results

Metabolism of ¹²³I-IMZ in vitro

We confirmed that the rates of flow (Rf) for ¹²³I⁻, ¹²³I-R-COOH, and ¹²³I-IMZ were in the ranges of 0.00–0.05, 0.40–0.50, and 0.95–1.00, respectively (Fig. 1). Figure 2 shows metabolite analyses of ¹²³I-IMZ with and without BNPP. The fractional ratio of ¹²³I-R-COOH decreased from 44 to 2%, whereas that of ¹²³I-IMZ increased from 44 to 89%, depending on the BNPP concentration. Figure 3 shows metabolite analyses of ¹²³I-IMZ with and without NADPH generator. With NADPH generator, we confirmed fractions of ¹²³I-R-COOH, an unknown metabolite [metabolite 2 (M2)], ¹²³I⁻, and ¹²³I-IMZ, whereas without NADPH generator, the only fraction not detected was M2.

Whole-body imaging and biological distribution in normal mice using ^{123/125}I-IMZ

Whole-body SPECT images were acquired using three normal mice, and similar images were obtained. Figure 4 shows whole-body images of a mouse at 15, 30, and 60 min after injection of ¹²³I-IMZ. At 15 min after injection, ¹²³I-IMZ primarily accumulated in the brain, liver, and kidney. At

30 min, accumulation in the liver decreased, whereas accumulation in the thyroid and bladder increased. At 60 min, significant ^{123}I -IMZ accumulation in the gall bladder, intestine, and bladder was noted. Table 1 shows the biological distribution in normal mice using ^{125}I -IMZ. Radioactivity in the lung, liver, kidney, and blood rapidly increased immediately after injection and then gradually decreased. In the thyroid, gall bladder, small intestine, and bladder, radioactivity gradually increased after injection.

Whole-body imaging and biological distribution in mice administered BNPP using $^{123/125}\text{I}$ -IMZ

Figure 5 shows whole-body images of a mouse administered 100 mg/kg BNPP at 15, 30, and 60 min after injection of ^{123}I -IMZ. In three mice, similar whole-body images were obtained. At 15 min after injection, ^{123}I -IMZ mainly accumulated in the brain and liver. At 30 min, accumulation in the liver slightly decreased, whereas accumulation in the intestine and bladder increased. At 60 min, ^{123}I -IMZ gradually accumulated in the gall bladder and intestine.

Table 2 shows the biological distribution in mice administered 50 or 100 mg/kg BNPP at 30, 60, and 120 min after ^{125}I -IMZ injection. Accumulation in the brain and liver significantly increased with administration of 100 mg/kg BNPP compared with normal mice at 30 min after ^{125}I -IMZ injection, whereas accumulation in the thyroid, lung, heart, stomach, gall bladder, and small intestine significantly decreased. The effect of 100 mg/kg BNPP was greater than that of 50 mg/kg BNPP. Accumulation

in the blood and urine was varied, compared with normal mice, because of the effect of BNPP.

Metabolism of ^{123}I -IMZ in vivo

Figure 6a–d shows metabolite analyses in the plasma, liver, bile, and urine, respectively. In the plasma, fractions of ^{123}I -R-COOH and $^{123}\text{I}^-$ were found. At 10 min after injection, ^{123}I -IMZ was metabolized to 70% ^{123}I -R-COOH and 26% $^{123}\text{I}^-$. The fractional ratio of ^{123}I -R-COOH gradually decreased to 14% at 120 min after injection, whereas that of $^{123}\text{I}^-$ significantly increased to 77%. In the liver, we confirmed fractions of ^{123}I -R-COOH, two unknown metabolites [metabolite 1 (M1) and M2], $^{123}\text{I}^-$, and ^{123}I -IMZ. The Rf values for M1 and M2 were in the ranges of 0.20–0.30 and 0.75–0.80, respectively. At 10 min after injection, the fractional ratios of ^{123}I -R-COOH, M1, M2, $^{123}\text{I}^-$, and ^{123}I -IMZ were 72, 0.9, 3, 17, and 2%, respectively. The fractional ratios of ^{123}I -R-COOH and ^{123}I -IMZ decreased to 24 and 4%, respectively, at 120 min after injection, whereas that of $^{123}\text{I}^-$ significantly increased to 60%. In the bile, the fractional ratios of ^{123}I -R-COOH, M1, M2, $^{123}\text{I}^-$, and ^{123}I -IMZ were 70, 6, 0.8, 14, and 3%, respectively, at 10 min after injection. The fractional ratios of ^{123}I -R-COOH and ^{123}I -IMZ slightly decreased to 63 and 0%, respectively, at 120 min after injection, whereas that of $^{123}\text{I}^-$ slightly increased to 25%. The other fractional ratios remained relatively unchanged. In the urine, the fractional ratios of ^{123}I -R-COOH, M1, M2, $^{123}\text{I}^-$, and ^{123}I -IMZ were 84, 4, 0.6, 5, and 0%, respectively, at 10 min after injection. The fractional ratio of ^{123}I -R-COOH slightly decreased to 78% at 120 min after injection, whereas that of $^{123}\text{I}^-$

slightly increased to 10%. The other fractional ratios remained relatively unchanged.

Discussion

Nuclear medicine imaging provides higher sensitivity and quantification capability to detect the activity of hepatic drug-metabolizing enzymes compared with other imaging techniques. Although radiopharmaceuticals are typically highly stable over time in vivo, our methodology indicates that they are almost fully metabolized in the liver, with metabolites accumulating in the excretory organs. Using this pathway for the metabolism of ^{123}I -IMZ, which Yoshimura et al. [16] described, the present study investigated direct, noninvasive detection and quantification of the activity of hepatic drug-metabolizing enzymes using ^{123}I -IMZ whole-body imaging.

Metabolism of ^{123}I -IMZ in vitro

Although the metabolic pathway and the TLC Rf values of ^{123}I -IMZ was previously reported [16,17], TLC Rf values for ^{123}I -R-COOH-Glc and ^{123}I -R'-CH₂COOH were not provided, and the authors could not detect the hepatic drug-metabolizing enzymes A and B (Supplementary Fig., Supplemental digital content 1, <http://links.lww.com/NMC/A132>). The TLC analyses of the present study demonstrated that ^{123}I -IMZ was metabolized to ^{123}I -R-COOH, $^{123}\text{I}^-$, and two unknown metabolites (M1 and M2). We then attempted to identify enzyme A (which converted ^{123}I -IMZ to ^{123}I -R-COOH) and enzyme B

(which converted ^{123}I -IMZ to M2). In the presence of BNPP, a specific and hepatic carboxylesterase inhibitor (Fig. 2), BNPP causes reduction of enzyme activity on hepatic carboxylesterase [21,24]. The fractional ratio of ^{123}I -R-COOH decreased depending on the concentration of BNPP, whereas the fractional ratio of ^{123}I -IMZ increased, and other metabolites remained relatively unchanged. These results confirm that enzyme A is carboxylesterase. In the event of carboxylesterase dysfunction in the liver, production of ^{123}I -R-COOH would be inadequate. Carboxylesterase plays an important role in the metabolism of ester-containing drugs and prodrugs [25] such as temocapril, angiotensin-converting-enzyme inhibitor [26], irinotecan, antitumor drugs [27], and cocaine-based narcotics [28]. Thus, it is an extremely important hepatic drug-metabolizing enzyme in humans. In the absence of NADPH generator to provide energy for CYP, M2 was not detected (Fig. 3). Therefore, we concluded that enzyme B, which converts ^{123}I -IMZ to M2, was CYP. However, it appears that CYP plays a less significant role in the metabolism of ^{123}I -IMZ than carboxylesterase, because only small amounts of M2 were detected in the analysis of in-vivo metabolism of ^{123}I -IMZ (Fig. 3). Therefore, based on CYP dependence, we conclude that M2 is ^{123}I -R'-CH₂COOH, and the remaining M1 would be ^{123}I -R-COOH-Glc (Supplementary Fig., Supplemental digital content 1, <http://links.lww.com/NMC/A132>).

Whole-body imaging and biological distribution in normal mice using $^{123}/^{125}\text{I}$ -IMZ

To directly detect and quantify the activity of drug-metabolizing enzymes in metabolic drug clearance, it is necessary to image and quantify the accumulation of the enzymes in the excretory organ. In whole-body imaging (Fig. 4) and analyses of the biological distribution of ^{125}I -IMZ (Table 1), $^{123/125}\text{I}$ -IMZ radioactivity was high in the blood, lung, liver (metabolic organ), and kidney (excretory organ) immediately after injection. This accumulation of radioactivity decreased over time. We can also confirm accumulation of radioactivity in the brain, the target organ of $^{123/125}\text{I}$ -IMZ. By contrast, radioactivity in the thyroid, gall bladder, small intestine, and bladder increased over time. These data indicate that ^{123}I -IMZ is excreted by enterohepatic and renal routes, as previously reported [17–19]. In addition, we found that $^{123/125}\text{I}$ -IMZ is metabolized to $^{123/125}\text{I}^-$ based on accumulation in the thyroid; however, $^{123/125}\text{I}^-$ radioactivity in the thyroid was much lower than that in the gall bladder and bladder.

Whole-body imaging and biological distribution in mice administered BNPP using $^{123/125}\text{I}$ -IMZ

Model mice with reduction of enzyme activity on carboxylesterase were produced by intraperitoneal BNPP injection. Changes in accumulation throughout the whole body were found in mice administered BNPP (Fig. 5 and Table 2). Especially, the accumulation in the brain, gall bladder, intestine and bladder was lower than that of a normal mouse (Fig. 4), whereas the accumulation in the liver was higher than that of a normal mouse, although color scales were the same between a normal mouse and a mouse

administered BNPP.

In biological distribution, accumulation in the liver significantly increased depending on the concentration of BNPP compared with normal mice (Fig. 4 and Table 1), whereas accumulation in the gall bladder and small intestine significantly decreased at 30 and 60 min after ^{125}I -IMZ injection. ^{125}I -IMZ accumulation in the gall bladder decreased by less than half in comparison with normal mice, whereas that in the liver increased by about two times in 50 and 100 mg/kg BNPP loading. BNPP is surmised to mainly inhibit hepatic carboxylesterase activity converting ^{125}I -IMZ to ^{125}I -R-COOH, although the BNPP-induced reduction in hepatic carboxylesterase activity should be evaluated by an enzyme assay with the appropriate substrate or western blot analysis. Furthermore, although we have to confirm the changes in metabolites of ^{125}I -IMZ by TLC analysis, M2, ^{125}I -IMZ and/or $^{125}\text{I}^-$ would accumulate in the gall bladder and small intestine in mice administered BNPP. The effect of BNPP can also be confirmed by the lower accumulation in the brain of mice administered BNPP compared with normal mice (Tables 1 and 2), because BNPP would inhibit cerebral carboxylesterase activity. However, accumulation in the blood and urine was varied compared with normal mice, because blood and the bladder are susceptible to the effect of BNPP. Thus, if enzyme activity of hepatic carboxylesterase is reduced by hepatic dysfunction caused by some influence of medicine or diseases etc., in the clinical study, the ^{123}I -IMZ imaging may provide evidence of higher accumulation in the liver and lower accumulation in the gall bladder and bladder for the direct measurement of the activity of hepatic carboxylesterase

in comparison with healthy subjects.

Metabolism of ^{123}I -IMZ in vivo

To directly detect and quantify the activity of drug-metabolizing enzymes in metabolic drug clearance, the radioactive metabolites of ^{123}I -IMZ need to move from a metabolic organ to an excretory organ early. Figure 6a shows that the ^{123}I -R-COOH and $^{123}\text{I}^-$ fractions were primarily found in the plasma. The fractional ratio of ^{123}I -R-COOH gradually decreased over time, whereas that of $^{123}\text{I}^-$ increased, possibly because of deiodinase activity in the organs (e.g. liver and kidney). The fractions differed in the liver, bile, and urine. The fractions in the plasma could reflect whole-body conditions. Therefore, we believe that the results of TLC analyses of blood samples do not only reflect hepatic metabolites. In the liver (Fig. 6b), the fractional ratio of ^{123}I -R-COOH peaked immediately after injection. Over time, the fractional ratio of ^{123}I -R-COOH decreased, whereas that of $^{123}\text{I}^-$ increased. Small amounts of other fractions (M1, M2, and ^{123}I -IMZ) were also detected. Some of the metabolites in the liver shifted to bile in the gall bladder (Fig. 6c) and to urine in the bladder (Fig. 6d). In the bile and urine, the fractional ratios of all metabolites were similar and remained stable at all of the time points examined. In particular, ^{123}I -R-COOH exhibited the highest fractional ratio (about 70% in the bile and 84% in the urine) of all metabolites. Other metabolites, including $^{123}\text{I}^-$, exhibited significantly lower fractional ratios than ^{123}I -R-COOH. Little or no administered ^{123}I -IMZ was found in the bile and urine by enterohepatic and renal routes. With regard to hepatic

carboxylesterase in the metabolic conversion of $^{123}\text{I-IMZ}$ to $^{123}\text{I-R-COOH}$ (Supplementary Fig., Supplemental digital content 1, <http://links.lww.com/NMC/A132>), the activity of hepatic carboxylesterase could be detected on the basis of accumulation of radioactivity in the gall bladder through the bile and the bladder through the urine in $^{123}\text{I-IMZ}$ whole-body imaging (Figs 4 and 5 and Tables 1 and 2).

Limitations

$^{123}\text{I-IMZ}$ whole-body imaging targeting the gall bladder or bladder may enable the measurement of individual variations in carboxylesterase activity. Following confirmation of the utility of $^{123}\text{I-IMZ}$ whole-body imaging, our novel methodology should be evaluated in clinical studies after passing a clinical ethical review with the results of this study, although extreme care must be taken with regard to the number and types of metabolites examined, because Yoshimura et al. [15] suggested that there were slight differences in metabolites between animals and humans. For example, low levels of a hydrolysis metabolite ($^{123}\text{I-R}'\text{-OH}$) of $^{123}\text{I-IMZ}$ have been detected in rats and rabbits, but not in mice or humans. Although we identified M2 as $^{123}\text{I-R}'\text{-CH}_2\text{COOH}$ in this study, $^{123}\text{I-R}'\text{-OH}$ may also be CYP dependent because of the hydrolysis metabolite. However, this would not affect the identification of enzyme B (which converts $^{123}\text{I-IMZ}$ to M2) as CYP.

Conclusions

As preliminary study for clinical application, $^{123}\text{I-IMZ}$ whole-body

imaging has good possibility of the direct measurement of the activity of hepatic carboxylesterase, which converted $^{123}\text{I-IMZ}$ to $^{123}\text{I-R-COOH}$, as determined by the accumulation of $^{123}\text{I-R-COOH}$ in the gall bladder and in the bladder. This novel $^{123}\text{I-IMZ}$ whole-body imaging methodology might be useful in determining the dosage of drugs to use in clinical individualized medicine.

Financial disclosure

This study was funded in part by Grants-in-Aid for Scientific Research from the Japan Society for the Promotion of Science (Nos. 25293260, 15K09949, and 15K15452, and 16KK0200).

Disclaimer

There are no conflicts of interest.

Acknowledgments

The author would like to thank Mikie Ohtaki and the other laboratory staff of Kanazawa University.

Supplemental Digital Content

Supplemental Digital Content 1.docx

References

- 1 Singh D, Kashyap A, Pandey RV, Saini KS. Novel advances in

cytochrome P450 research. *Drug Discov Today* 2011; 16:793–799.

2 Ross MK, Borazjani A, Wang R, Crow JA, Xie S. Examination of the carboxylesterase phenotype in human liver. *Arch Biochem Biophys* 2012; 522:44–56.

3 Ingelman-Sundberg M, Oscarson M, McLellan RA. Polymorphic human cytochrome P450 enzymes: an opportunity for individualized drug treatment. *Trends Pharmacol Sci* 1999; 20:342–349.

4 Rogers JF, Nafziger AN, Bertino JS, Jr. Pharmacogenetics affects dosing, efficacy, and toxicity of cytochrome P450-metabolized drugs. *Am J Med* 2002; 113:746–750.

5 Laizure SC, Herring V, Hu Z, Witbrodt K, Parker RB. The role of human carboxylesterases in drug metabolism: have we overlooked their importance? *Pharmacotherapy* 2013; 33:210–222.

6 Reed JR, Backes WL. Formation of P450 • P450 complexes and their effect on P450 function. *Pharmacol Ther* 2012; 133:299–310.

7 Hosokawa M, Endo T, Fujisawa M, Hara S, Iwata N, Sato Y, et al. Interindividual variation in carboxylesterase levels in human liver microsomes. *Drug Metab Dispos* 1995; 23:1022–1027.

8 Imai T, Taketani M, Shii M, Hosokawa M, Chiba K. Substrate specificity of carboxylesterase isozymes and their contribution to hydrolase activity in human liver and small intestine. *Drug Metab Dispos* 2006; 34:1734–1741.

9 Watkins PB. Noninvasive tests of CYP3A enzymes. *Pharmacogenetics*

1994; 4:171–184.

10 Chiba M, Ishii Y, Sugiyama Y. Prediction of hepatic clearance in human from in vitro data for successful drug development. *AAPS J* 2009; 11:262–276.

11 Cohen MB, Graham LS, Yamada LS. ¹²³Iodoamphetamine SPECT imaging. *Int J Rad Appl Instrum A* 1986; 37:749–763.

12 Mimura H, Sone T, Takahashi Y, Yoshioka K, Murase K, Matsuda H, et al. Measurement of regional cerebral blood flow with ¹²³I-IMP using one-point venous blood sampling and causality analysis: evaluation by comparison with conventional continuous arterial blood sampling. *Ann Nucl Med* 2006; 20:589–595.

13 Fujita K, Sugiyama M, Akiyama Y, Hioki K, Kunishima M, Nishi K, et al.

N-Isopropyl-p-iodoamphetamine hydrochloride is predominantly metabolized by CYP2C19. *Drug Metab Dispos* 2012; 40:843–846.

14 Nishi K, Mizutani A, Shikano N, Fujita K, Kobayashi M, Ono M, et al. In vivo radioactive metabolite analysis for individualized medicine: A basic study of a new method of CYP activity assay using ¹²³I-IMP. *Nucl Med Biol* 2015; 42:171–176.

15 Holl K, Deisenhammer E, Dauth J, Carmann H, Schubiger PA. Imaging benzodiazepine receptors in the human brain by single photon emission computed tomography (SPECT). *Int J Rad Appl Instrum B* 1989; 16:759–763.

16 Yoshimura H, Yanai A, Matsumoto H, Ida K, Kurami M, Yonekura Y,

et al.

Pharmacokinetics of ^{123}I -iomazenil, a benzodiazepine receptor seeker. *Kaku Igaku* 1995; 32:1037–1043.

17 Zoghbi SS, Baldwin RM, Seibyl JP, al-Tikriti MS, Zea-Ponce Y, Laruelle M, et al. Pharmacokinetics of the SPECT benzodiazepine receptor radioligand ^{123}I iomazenil in human and non-human primates. *Int J Rad Appl Instrum B* 1992; 19:881–888. 18 Verhoeff NP, Busemann Sokole E, Hengst D, Stubbs JB, van Royen EA. Dosimetry of iodine-123 iomazenil in humans. *Eur J Nucl Med* 1993; 20:580–584.

19 Dey HM, Seibyl JP, Stubbs JB, Zoghbi SS, Baldwin RM, Smith EO, et al. Human biodistribution and dosimetry of the SPECT benzodiazepine receptor radioligand iodine-123-iomazenil. *J Nucl Med* 1994; 35:399–404.

20 Smith PK, Krohn RI, Hermanson GT, Mallia AK, Gartner FH, Provenzano MD, et al.

Measurement of protein using bicinchoninic acid. *Anal Biochem* 1985; 150:76–85. 21 Heymann E, Krisch K. Phosphoric acid-bis-(p-nitrophenylester), a new inhibitor of microsomal carboxylesterases. *Hoppe Seylers Z Physiol Chem* 1967; 348:609–619.

22 Deimling OV, Bocking A. Esterases in histochemistry and ultrahistochemistry. *Histochem J* 1976; 8:215–222.

23 Beer HF, Blauenstein PA, Hasler PH, Delaloye B, Riccabona G, Bangerl I, et al. In vitro and in vivo evaluation of iodine-123-Ro 16-0154: a new imaging agent for SPECT investigations of benzodiazepine receptors. *J Nucl Med* 1990; 31:1007–1014.

- 24 Ahmed S, Imai T, Otagiri M. Evaluation of stereoselective transdermal transport and concurrent cutaneous hydrolysis of several ester prodrugs of propranolol: mechanism of stereoselective permeation. *Pharm Res* 1996; 13:1524–1529.
- 25 Takai S, Matsuda A, Usami Y, Adachi T, Sugiyama T, Katagiri Y, et al. Hydrolytic profile for ester- or amide-linkage by carboxylesterases pI 5.3 and 4.5 from human liver. *Biol Pharm Bull* 1997; 20:869–873.
- 26 Humerickhouse R, Lohrbach K, Li L, Bosron WF, Dolan ME. Characterization of CPT-11 hydrolysis by human liver carboxylesterase isoforms hCE-1 and hCE-2. *Cancer Res* 2000; 60:1189–1192.
- 27 Pindel EV, Kedishvili NY, Abraham TL, Brzenzinski MR, Zhang J, Dean RA, et al. Purification and cloning of a broad substrate specificity human liver carboxylesterase that catalyzes the hydrolysis of cocaine and heroin. *J Biol Chem* 1997; 272:14769–14775.

Figure legends

Fig. 1. Thin-layer chromatography analysis of radioactivity in plasma (a), liver (b), bile (c), and urine (d) samples. Samples were obtained from mice at 10, 30, 60, and 120 min after ^{123}I -Iomazenil (^{123}I -IMZ) injection. Relative radioactivity was calculated by dividing the radioactive counts for each fraction by the total radioactivity. Rf values for $^{123/125}\text{I}$, $^{123/125}\text{I}$ -R-COOH, and $^{123/125}\text{I}$ -IMZ were in the ranges of 0.00–0.05, 0.40–0.50, and 0.95–1.00, respectively. In addition, Rf values for other unknown metabolites [metabolite

1 (M1) and metabolite 2 (M2)] were 0.20–0.30 and 0.75–0.80, respectively.

Fig. 2. In-vitro analysis of metabolites of ^{123}I -Iomazenil (^{123}I -IMZ) with and without bis(4-nitrophenyl) phosphate (BNPP). The percent radioactivity of each sample was determined using mouse liver homogenate without BNPP (0 $\mu\text{mol/l}$) or with 0.1, 1, 10, or 100 $\mu\text{mol/l}$ BNPP. Error bars indicate the SD.

Fig. 3. In-vitro analysis of metabolites of ^{123}I -Iomazenil (^{123}I -IMZ) with and without nicotinamide adenine dinucleotide phosphate (NADPH) generator. The percent radioactivity of each sample was determined using mouse liver homogenate with NADPH generator [NADPH (+)] or without NADPH generator [NADPH ()]. Error bars indicate the SD.

Fig. 4. Whole-body images of a mouse obtained 15, 30, and 60 min after 45 MBq ^{123}I -Iomazenil (^{123}I -IMZ) injection under 2.0% isoflurane anesthesia. Acquisition time was 3 min from the start time in each scan.

Fig. 5 Whole-body images of a mouse administered 100 mg/kg bis(4-nitrophenyl) phosphate obtained 15, 30, and 60 min after 45 MBq ^{123}I -Iomazenil (^{123}I -IMZ) injection under 2.0% isoflurane anesthesia. Acquisition time was 3 min from the start time in each scan.

Fig. 6. In-vivo analysis of three normal mice of metabolites in plasma (a), liver (b), bile (c), and urine (d). The percent radioactivity of each sample was

determined from three mice at 10, 30, 60, and 120 min after ^{123}I -Iomazenil (^{123}I -IMZ) injection. Error bars indicate the SD.

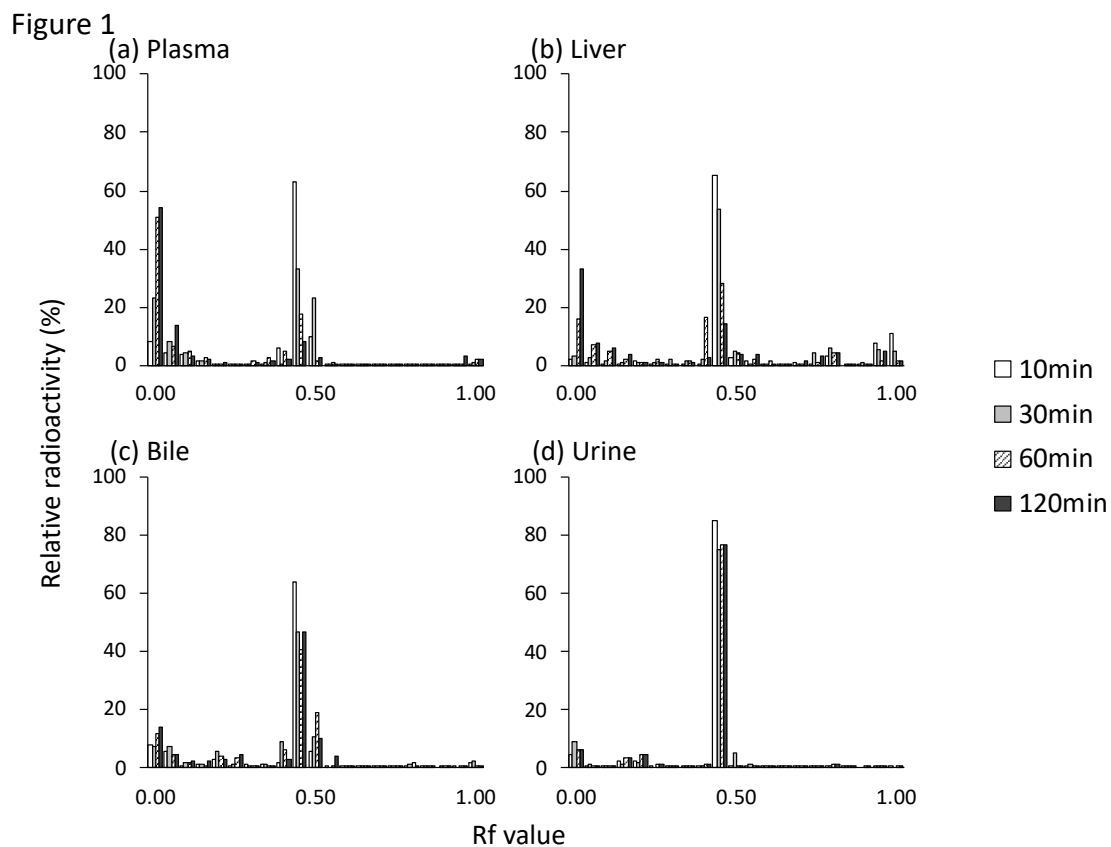


Figure 2

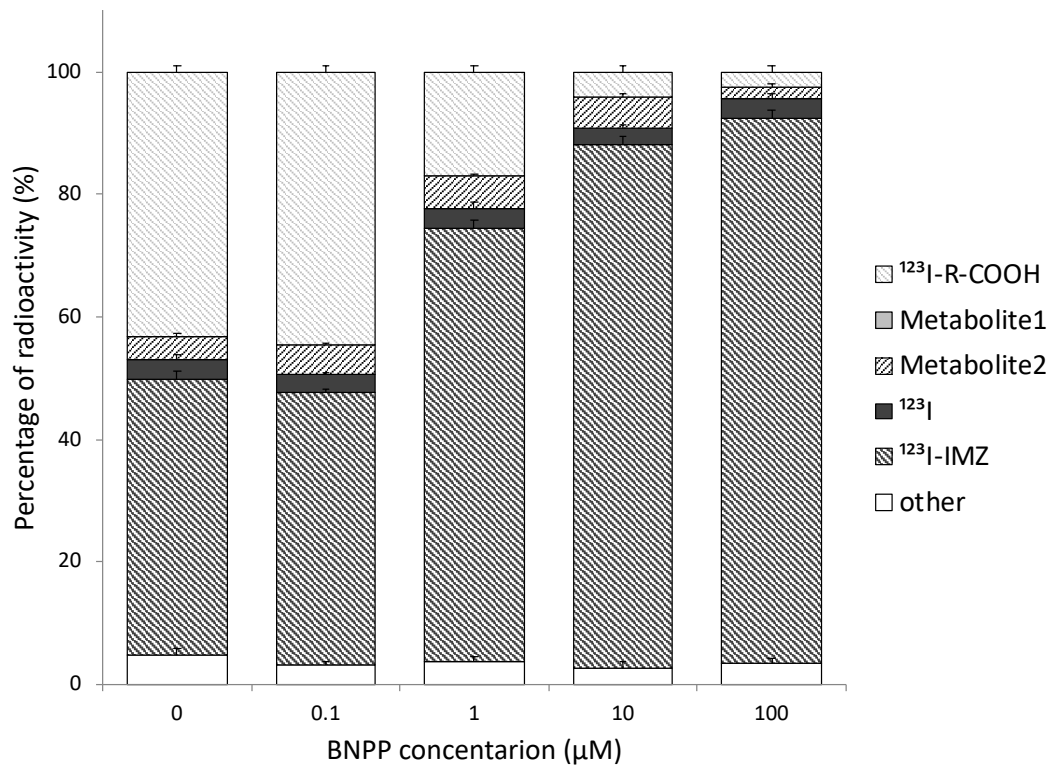


Figure 3

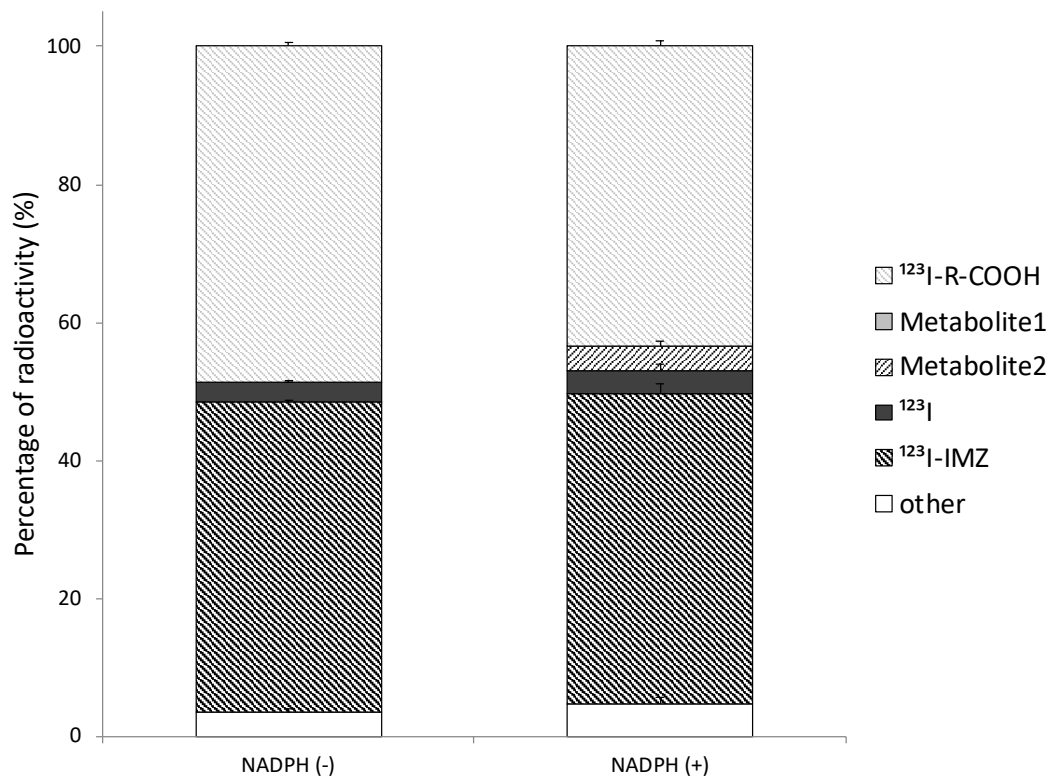


Figure 4

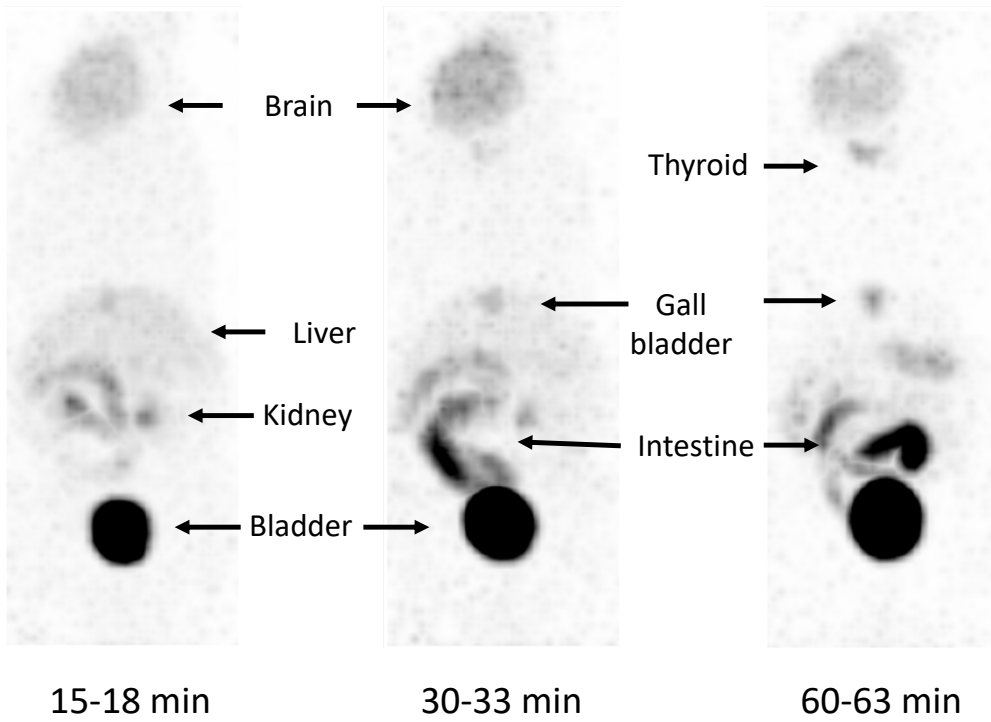


Figure 5

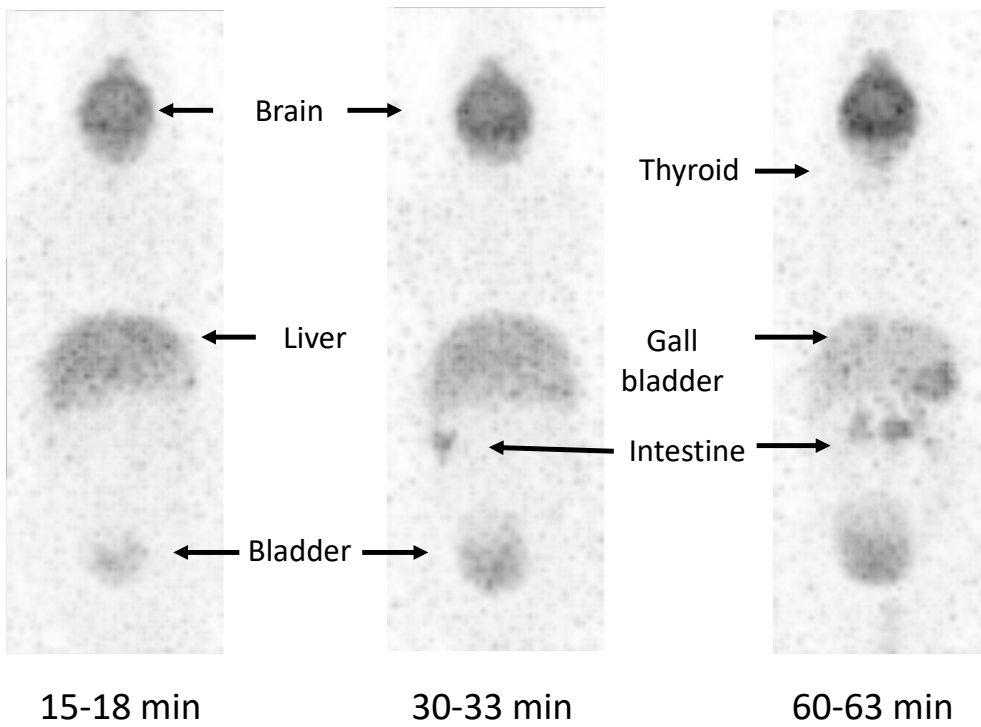


Figure 6

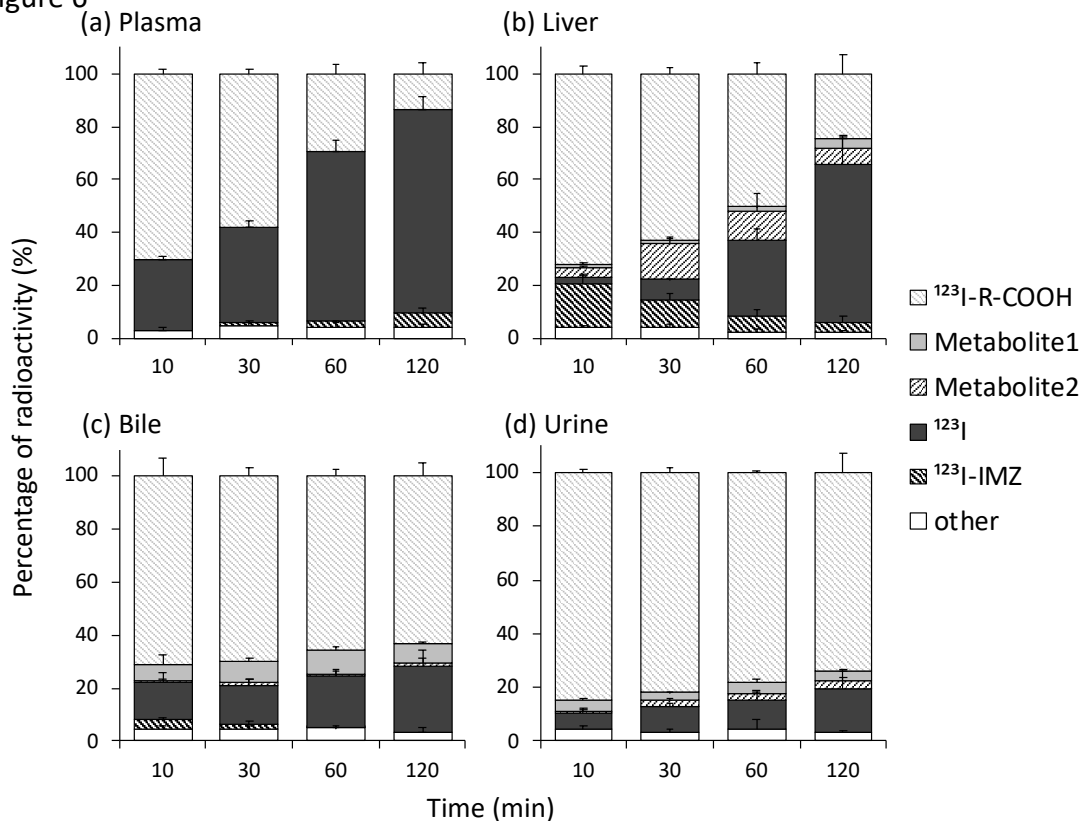


Table.1

Organ	Time (min)					
	2	5	10	30	60	120
Blood	6.82 ± 0.11	5.55 ± 0.58	4.27 ± 0.34	2.77 ± 0.14	1.85 ± 0.36	1.91 ± 0.20
Brain	3.95 ± 0.42	5.19 ± 1.15	4.40 ± 0.26	3.58 ± 0.41	2.10 ± 0.40	1.38 ± 0.06
Thyroid*	0.47 ± 0.13	0.55 ± 0.06	0.70 ± 0.12	1.53 ± 0.12	2.72 ± 0.47	3.60 ± 0.62
Lung	6.06 ± 0.27	5.11 ± 0.65	3.86 ± 0.34	2.31 ± 0.09	1.47 ± 0.29	1.46 ± 0.11
Heart	4.44 ± 0.19	3.73 ± 0.61	2.86 ± 0.23	1.96 ± 0.31	1.24 ± 0.19	1.21 ± 0.04
Stomach*	2.96 ± 0.59	5.06 ± 1.43	6.97 ± 0.31	11.86 ± 2.11	10.14 ± 1.95	8.32 ± 2.74
Liver	11.34 ± 1.76	11.30 ± 1.34	8.15 ± 0.82	3.16 ± 0.16	1.35 ± 0.37	1.20 ± 0.05
Gall bladder	4.75 ± 1.06	9.06 ± 5.59	9.09 ± 4.92	57.27 ± 6.59	76.69 ± 7.30	46.67 ± 3.56
Small intestine*	6.93 ± 0.44	8.24 ± 0.57	9.32 ± 1.09	12.79 ± 1.43	17.00 ± 3.56	10.50 ± 4.02
Large intestine*	2.34 ± 0.13	1.93 ± 0.05	1.68 ± 0.24	1.52 ± 0.23	1.09 ± 0.21	2.94 ± 3.23
Kidney	12.58 ± 1.76	11.61 ± 2.43	10.78 ± 5.07	6.07 ± 3.43	3.61 ± 2.17	5.02 ± 3.52
Urine*	0.78 ± 1.07	3.55 ± 3.11	10.99 ± 3.41	13.25 ± 9.37	32.43 ± 5.89	34.22 ± 3.28

Supplemental fig. 1

